COMPUTATIONAL PROBLEMS OF ELECTRICAL ENGINEERING

Vol. 3, No. 2, 2013

AN ANATOMICALLY REALISTIC BOUNDARY REPRESENTATION PHANTOM FOR STUDYING VHF–UHF RADIATION EFFECTS

Denys Nikolayev

Department of Theory of Electrical Engineering, University of West Bohemia, Pilzen, Czech Republic;
Lviv Polytechnic National University, Lviv, Ukraine
d@deniq.com

Abstract: Both ionizing and non-ionizing radiation dosimetry studies, medical imaging technologies, and image reconstruction algorithms require computational phantoms to assess health effects, to analyze efficiency and to test algorithms. The goal of this study is to overview existing models of a human body and to develop the anatomically realistic boundary representation phantom for VHF–UHF electromagnetic and coupled field studies. We use simulated magnetic resonance images as the source of the phantom geometry. One of the possible applications is illustrated by an example of coupled electric/thermal field distribution. Developed phantoms have a broad application in various branches of science and technology.

Key words: head phantom, boundary representation (B-Rep), radiofrequency, non-ionizing radiation, bioheat transfer, finite element method.

1. Introduction

Most of technology achievements of the last decades—cellular phones and laptops in our everyday environments, security gates in airports and anti-theft systems in malls, magnetic resonance imaging and wireless implants—expose human body to a radiofrequency electromagnetic field. To test these systems, to optimize their performance or to study the impact on health, we employ anthropomorphic human models, or *phantoms*; in vivo studies on humans are uncommon due to health hazards, ethical issues, and are impossible for the most cases. The term phantom comes from radiobiology and means the physical or mathematical model of a human body [1].

The special case is the radiation in VHF–UHF ranges where the radio waves of wavelength λ could be resonant within a human body or its internal organs with the linear dimensions a, so that

$$a / \lambda \cong 1. \qquad (1)$$

The objectives of this study are: 1) to overview existing phantoms and their limitations; 2) to develop a novel computationally efficient B-Rep phantom with anatomically realistic geometry required to study field distributions, propagation and resonance effects within a human head in VHF–UHF ranges.

2. Types of phantoms

Phantoms can be *physical* or *computational*. Computational ones consist of three generations: I — stylized anthropomorphic phantoms; II — voxel phantoms; III — boundary representation (B-Rep) phantoms, or CAD phantoms. B-Rep phantoms could be either of a polygonal or non-uniform rational basis spline (NURBS) type.

A. Physical phantoms

The *physical phantom* is made of a solid shell filled with liquid that has electrical properties close to real biological tissue. One example of a physical phantom is a specific anthropomorphic mannequin (SAM) on Fig. 1, which is specified by IEEE Std. 1528-2013 [2] and IEC 62209-1 [3], and is used for evaluating near-field exposure to wireless devices used in close proximity to a head. To study field distributions inside a physical phantom, it needs field probes mounted inside, affecting the field distributions and hence the results. Electric parameters of the phantom are averaged and homogenized: it introduces additional errors, especially on frequencies more than 400 MHz [4], [5]. Other drawbacks manifest themselves in expensive and time-consuming experiments [1].

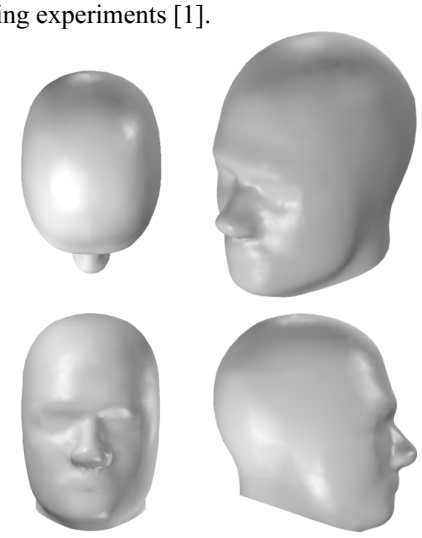

Fig. 1. Visualization of specific anthropomorphic mannequin (SAM) geometry, specified by IEEE and IEA as a physical phantom for evaluating near-field RF exposure.

B. Computational phantoms

First-generation computational phantoms were used *c*. 1940s for ionized radiation research and represented a homogeneous sphere or a cylinder. First heterogeneous phantoms roughly imitated the structure of a tissue; an example is Shepp–Logan phantom [6], widely employed in medical imaging (Fig. 2: left). Medical Internal Radiation Dose (MIRD) phantom (Fig. 2: right) was the first *stylized* anthropomorphic model of human anatomy [7]; its variations are still used today for ionizing radiation dosimetry employing Monte-Carlo method.

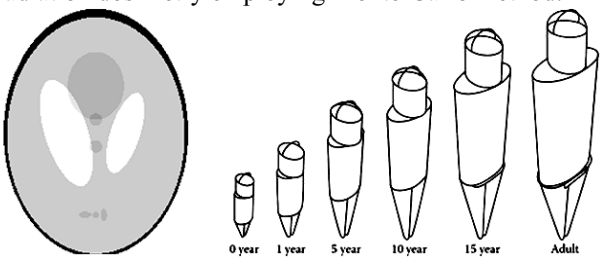

Fig. 2. First-generation computational phantoms. Left: Shepp–Logan phantom; right: "family" of stylized MIRD phantoms (Fisher and Snyder).

Second-generation computational phantoms or *voxel* phantoms were the first anatomically realistic models of a human body. They are based on cadaver cryosection photos from Visible Human Project [8], computed tomography (CT) and magnetic resonance imaging (MRI) scans. The up-to-date list of human voxel phantoms could be found in [1] and their comprehensive overview and comparison is given in [9]. Voxel phantoms are widely implemented for the SAR assessment; the most notable applications are in [10–13].

Voxel phantom development consists of three basic steps: 1) identifying tissues for every pixel on 2D raster images (photos, CT or MRI); 2) superposition of the sequence of segmented images into a 3D phantom; 3) assigning parameters of interest to voxels. The volume of a voxel is then defined as $V = Ah$, where A is the pixel area and h denotes the thickness of a slice.

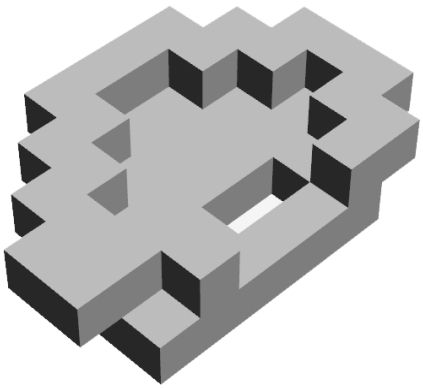

Fig. 3. Coarse voxel model of a human pinna (for illustrative purposes only).

Voxel phantoms soon became popular in non-ionizing radiation studies, since the field problems could be easily solved using finite-difference time-domain (FDTD) method. It is among the simplest and widely employed methods to be implemented for the full wave solution of Maxwell's equations [14].

The main drawbacks of voxel phantoms are the difficulty to deform and translate the geometry without considerable losses, "staircase effects" in the geometry [4] due to rotations, limited possibility for mesh space adaptivity [15], accordingly high computational costs and grow rate $O(N^3)$. For the analysis of propagation and resonance effects in human head in VHF–UHF range, the tissue boundary approximation in voxel phantoms is either inadequate or computationally inefficient.

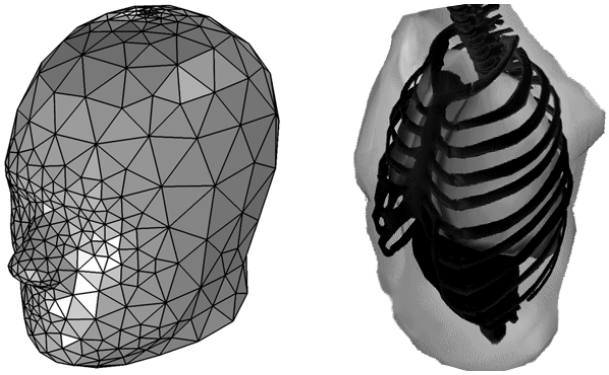

Fig. 4. B-Rep phantom examples. Left: Polygonal mesh representation of SAM; right: NCAT phantom.

Third-generation phantoms are boundary representation or B-rep phantoms. They do not have the drawbacks mentioned above. Either the polygonal mesh (Fig. 4: left) or the NURBS, (Fig. 4: right) approximate tissue boundaries, so it could be easily scaled, deformed or rotated without any loss. These phantoms are relatively new, the first versions were developed only after 2000 (NURBS-based cardiac-torso (NCAT) phantom [16]; Fig. 4: right). Till now they have been used primarily for ionizing radiation studies. The most prominent B-Rep phantoms used today for non-ionizing radiation are those of the Virtual Family group developed by Christ et al [15]. These phantoms are widely used for non-ionizing radiation exposure studies, notably in [17–19]. However, B-Rep phantoms are still often voxelized to carry out FDTD analysis, consequently reducing the computational efficiency or accuracy.

Polygonal mesh phantoms (Fig. 4: left) are the set of closed surfaces $\partial\Omega_i$ in $\mathbb{R}^3$ (or closed polygons $\partial\Gamma_i$ in $\mathbb{R}^2$ for 2D phantoms) representing the tissue boundaries. The surfaces $\partial\Omega_i$ consist of the set of polyhedrons (usually triangles)

$$F = \{f_1, f_2, \ldots f_k\}, \; f_i \in V \times V \times V, \qquad (2)$$

formed by the set of vertices

$$V = \{v_1, v_2, \ldots, v_n\}, \tag{3}$$

and the set of edges

$$E = \{e_1, e_2, \ldots e_m\}, \; e_i \in V \times V. \tag{4}$$

NURBS models the tissue by parametrically representing it with surfaces of degrees *p, q* in directions *u, v*. A simple NURBS curve is a polynomial function of the form [17]:

$$\mathbf{C}(u) = \frac{\sum_{i=0}^{n} w_i \mathbf{P}_i N_{i,p}(u)}{\sum_{i=0}^{n} w_i N_{i,p}(u)}, \tag{5}$$

where w_i are weights, $\mathbf{P}_i$ denotes the control points and $N_{i,p}(u)$ stands for the normalized B-spline basis function of degree p. NURBS surface is defined in a similar way.

The polygonal mesh could be easily converted to a NURBS model and vice versa using various 3D CAD packages. Modern research efforts are focused on the creation of new hybrid phantoms of the subjects of various ages and sexes for augmenting the statistical significance of simulation results.

Existing B-Rep phantoms are either not enough accurate for studying resonance effects in head tissues or containing too much details for computationally efficient finite element mesh. Therefore, the new phantom must be developed to meet the requirements of necessary anatomical accuracy and computational efficiency.

3. B-Rep phantom development

The building process of the B-Rep phantom consists of the following steps:

1. acquiring the subject slice data using MRI, CT, or cryosection photos;
2. segmenting of the images according to the tissue type using image processing algorithms;
3. vectorizing obtained closed segments using piecewise linear approximation or NURBS curves;
4. for 3D phantoms: constructing surfaces bounded by obtained loops using polygons or NURBS surfaces (distance between the slices should be sufficiently small to preserve small objects and reduce topological errors);
5. combining obtained closed surfaces (edges for 2D models) into a completed phantom;
6. assigning appropriate tissue properties to the volumes enclosed in the surfaces.

To study the electromagnetic resonant properties of a human head and its excitation, we used the simulated MRI scan of a normal brain from Aubert-Broche et al. [21]. This approach is more time-efficient and provides adequate anatomical accuracy, since the tissues are already segmented within the generated scans.

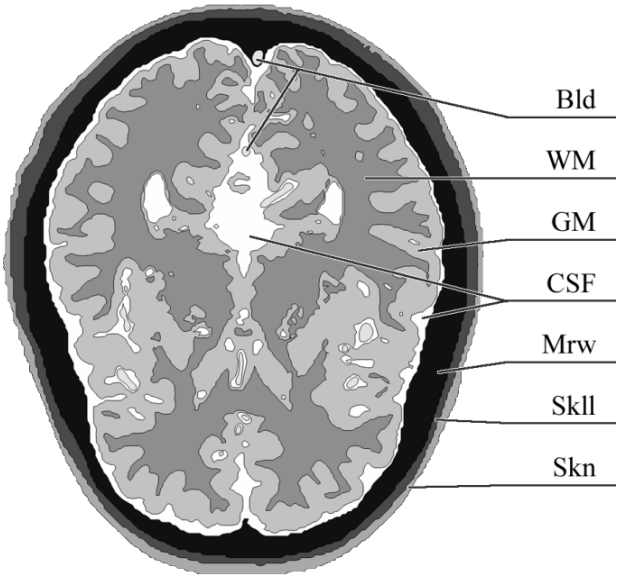

Fig. 5. Obtained 2D slice of B-Rep head phantom. Bld is blood; WM denotes white matter; GM means grey matter; CSF is cerebrospinal fluid; Mrw is bone marrow; Skll stands for a skull; Skn is skin.

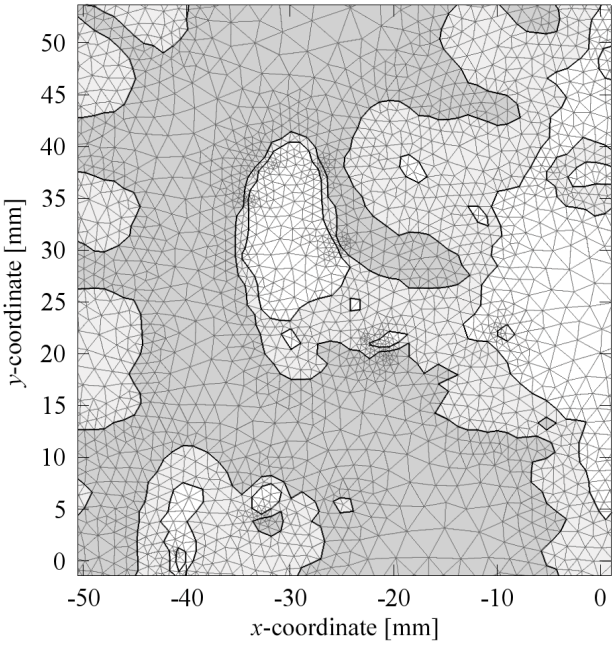

Fig. 6. Space-adaptive finite element mesh of the phantom.

For the vectorization of the images, we developed a MATLAB script that firstly reduces the color space by converting a raster image to indexed one (function `rgb2ind()`) and then traces region boundaries (using `bwboundaries()`). Now, boundaries could be converted to shapes using polygons or NURBS and combined to the final geometry (Fig. 5). Outer layers (Skll/Mrw) are simplified in order to reduce the number of degrees of freedom (DoF); the model can be still considered as realistic for field distribution studies and

remains adequate up to the frequency of about 2 GHz [5]. The electric properties of tissue were assigned according to the data from Gabriel et al [22] and the thermal ones are from Hasgall et al [23].

Finally, the phantom can be meshed using different types of adaptivity for achieving desired accuracy and performance. Fig. 6 shows the example of space-adaptive meshing of the resulted phantom. It could be clearly seen that FDTD meshing would produce much more DoF (and thus require more computational resource) to accurately describe the geometry of tissue boundaries.

4. Example of application: FEM analysis of coupled physical fields in a human head

We employed finite element method to study electromagnetic eigenfrequencies [5], resonance excitation and Specific Absorption Rate (SAR). COMSOL Multiphysics® and the in-house software Agros2D [24] was used for coupled field simulations.

To find electric field distributions, we use the standard harmonic wave function:

$$\nabla \times \frac{1}{\mu_r}\left(\nabla \times \mathbf{E}\right) - k_0^2\left(\varepsilon_r - \frac{j\sigma}{\omega\varepsilon_0}\right)\mathbf{E} = 0\,, \qquad (6)$$

where μ_r and ε_r are respectively relative permeability and relative permittivity, σ is the electrical conductivity [S/m], ω denotes the frequency [rad/s], and k_0 is the wave number of free space.

Perfectly matched layer (PML) was used in order to truncate the study region in combination with Dirichlet boundary condition to set the field to zero at the outer domain:

$$\mathbf{n} \times \mathbf{E} = 0. \qquad (7)$$

After solving (6) for electric field **E**, specific absorption rate distribution could be found using

$$\mathrm{SAR}\left(\mathbf{r}\right) = \int \frac{\sigma(\mathbf{r})\left|\mathbf{E}(\mathbf{r})\right|^2}{\rho(\mathbf{r})} d\mathbf{r}\,, \qquad (8)$$

where ρ is the tissue destiny [Kg/m^3], and **r** stands for the general space variable (*x, y* for the 2D phantom).

Fig. 7 shows the SAR distribution in a human head phantom due to incident plane wave propagating along *x*-axis in positive direction, i.e. left-to-right. SAR was computed from (8) after solving (6) for the **E** field.

From complex-valued field values (due to lossy materials) we can find the power dissipation density Q_e [W/m^3] [25]:

$$Q_e = \frac{1}{2}\mathrm{Re}\left(\mathbf{J} \cdot \hat{\mathbf{E}}\right) + \frac{1}{2}\mathrm{Re}\left(i\omega\mathbf{B} \cdot \hat{\mathbf{H}}\right), \qquad (9)$$

where the first term on the right-hand side represents the resistive losses and the second one stands for magnetic losses.

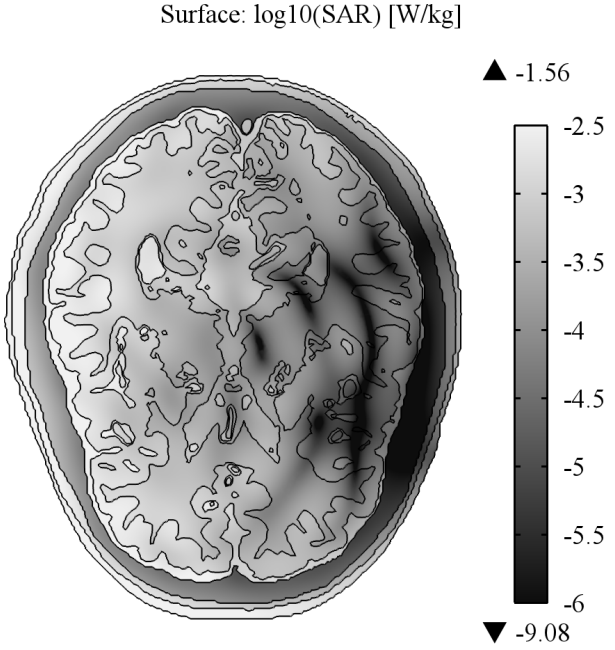

Fig. 7. SAR distribution in the developed human head phantom due to an incident plane wave propagating along x-axis (left-to-right).

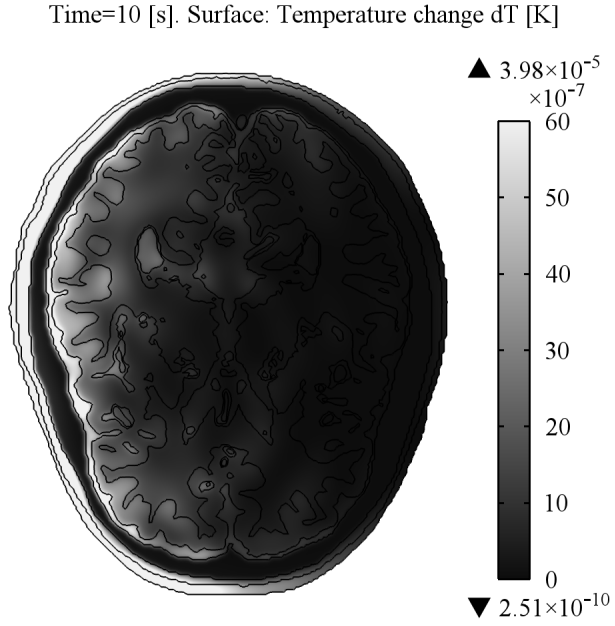

Fig. 8. Temperature change in the developed human head phantom after 10 seconds of exposure to incident plane wave propagating along x-axis (left-to-right).

Now we can assess the tissue heating process (without taking into account the blood flow) using the time dependent heat equation:

$$\rho C_p \frac{\partial T}{\partial t} - \nabla \cdot \left(k\nabla T\right) = Q_e\,, \qquad (10)$$

where k is the thermal conductivity of a tissue, C_p denotes the heat capacity and T is the temperature.

Neumann boundary condition must be applied in order to set the heat flux to zero at the limiting boundaries of the study domain:

$$-\mathbf{n}\cdot\left(-k\nabla T\right)=0. \tag{11}$$

Fig. 8 depicts the heating pattern of the tissue after 10 seconds of exposure to an incident plane wave (Fig. 7). One can clearly see the highly inhomogeneous distribution caused by the heterogeneous structure of a head tissue.

5. Discussion and conclusion

This study reviews and classifies the existing phantoms, describes the process of development of the new boundary representation phantom and provides an application example.

For the analysis of the problems involving full wave solutions of Maxwell's equations and containing optimization tasks, computational performance is essential. Moreover, we cannot oversimplify the geometry of a problem while studying the effects strongly affected by the structure of a head (e.g. SAR hotspots in a human head due to resonance effects that can arise due to RF exposure in VHF–UHF ranges). B-Rep phantoms provide the necessary anatomical accuracy for such tasks as well as it can take the full advantage of *hp*-adaptive finite element meshes increasing computational efficiency. B-rep phantoms could be also implemented with integral equation methods using boundary element discretization, but this approach was found generally inefficient for complex dielectric structures. Traditional approach using voxelization and FDTD method for computations is also possible and is widely implemented in modern software (e.g. SEMCAD X).

In this paper, a polygonal mesh based phantom was developed containing seven electrically and thermally distinct human head tissues with realistic anatomical structure. One of the possible applications of the phantom was demonstrated by an example of the FEM analysis of coupled physical fields—electromagnetic and thermal—using the mesh space adaptivity. The phantom could be used both for specific absorption assessment and wave propagation studies (e.g. for biomedical wireless implants). The development of the phantom is semi-automatic. Therefore, with the developed algorithm it is possible to vectorize the image data of necessary subject and create the anatomical models of other parts of the body, as well as the phantoms of animals.

The major limitation of the developed phantom is the anatomical precision due to the simple vectorization algorithm. However, obtained accuracy is sufficient to study coupled physical field distribution effects within a generalized human head in the defined frequency range. For resonance and propagation studies at the frequencies over 2 GHz, the outer layers of the phantom (skin-periosteum-skull-dura) must be refined. It could be done using the same algorithm providing higher resolution initial images.

The developed phantom can be widely applied in multi-branch studies. Apart from its primary usage in VHF–UHF radiation and coupled fields, it could be employed for the simulation of arbitrary field distributions and ionized radiation dosimetry.

Studies both ionizing/non-ionizing radiation dosimetry and in medical imaging are of the highest importance for the modern society. Providing the scientific community with new efficient computational phantoms contributes to the development of science, technology and health care.

Acknowledgments

This paper was supported by the project SGS-2012-039 (University of West Bohemia). Illustrations on Figures 2: right and 4: right are provided by Wikimedia Commons.

References

[1] X. G. Xu and K. F. Eckerman, *Handbook of Anatomical Models for Radiation Dosimetry*. Boca Raton, FL, USA: CRC Press, 2009.

[2] IEEE, "IEEE Recommended Practice for Determining the Peak Spatial-Average Specific Absorption Rate (SAR) in the Human Head from Wireless Communications Devices: Measurement Techniques," IEEE Std 1528-2013, 2013.

[3] IEC, "Human exposure to RF fields from hand-held and body-mounted wireless communication devices—Human models, instrumentation, and procedures—Part 1: Procedure to determine the SAR for hand-held devices used in close proximity to the ear (frequency range of 300 MHz to 3 GHz)," IEC 62209-1 ed 1.0, Feb. 2005.

[4] B. B. Beard, W. Kainz, T. Onishi, T. Iyama, S. Watanabe, O. Fujiwara, W. Jianqing, G. Bit-Babik, A. Faraone, J. Wiart, A. Christ, N. Kuster, L. Ae-Kyoung, H. Kroeze, M. Siegbahn, J. Keshvari, H. Abrishamkar, W. Simon, D. Manteuffel, and N. Nikoloski, "Comparisons of computed mobile phone induced SAR in the SAM phantom to that in anatomically correct models of the human head," *IEEE Trans. Electromagn. Compat.*, vol. 48, pp. 397–407, 2006.

[5] D. Nikolayev, "Radio Frequency Resonances inside a Human Head," *Comput. Probl. Electr. Eng.*, vol. 3, pp. 73-78, 2013.

[6] L. A. Shepp and B. F. Logan, "The Fourier reconstruction of a head section," *IEEE Trans. Nucl. Sci.*, vol. 21, no. 3, pp. 21–43, 1974.

[7] H. L. Fisher Jr and W. S. Snyder, "Variation of dose delivered by 137Cs as a function of body size from infancy to adulthood," *ORNL*, vol. 4007, pp. 221–228, 1966.

[8] M. J. Ackerman, "The visible human project," *Proc. IEEE*, vol. 86, no. 3, pp. 504–511, 1998.

[9] H. Zaidi and X. G. Xu, "Computational anthropomorphic models of the human anatomy: the path

to realistic Monte Carlo modeling in radiological sciences," *Annu Rev Biomed Eng*, vol. 9, pp. 471–500, 2007.

[10] P. J. Dimbylow and S. M. Mann, "SAR calculations in an anatomically realistic model of the head for mobile communication transceivers at 900 MHz and 1.8 GHz," *Phys. Med. Biol.*, vol. 39, pp. 1537–1553, 1994.

[11] C. M. Collins, W. Liu, J. Wang, R. Gruetter, J. T. Vaughan, K. Ugurbil, and M. B. Smith, "Temperature and SAR calculations for a human head within volume and surface coils at 64 and 300 MHz," *J. Magn. Reson. Imaging*, vol. 19, no. 5, pp. 650–656, 2004.

[12] B. B. Beard, W. Kainz, T. Onishi, T. Iyama, S. Watanabe, O. Fujiwara, W. Jianqing, G. Bit-Babik, A. Faraone, J. Wiart, A. Christ, N. Kuster, L. Ae-Kyoung, H. Kroeze, M. Siegbahn, J. Keshvari, H. Abrishamkar, W. Simon, D. Manteuffel, and N. Nikoloski, "Comparisons of computed mobile phone induced SAR in the SAM phantom to that in anatomically correct models of the human head," *IEEE Trans. Electromagn. Compat.*, vol. 48, pp. 397–407, 2006.

[13] E. Yakovenko and V. Goblyk, "The mathematical model of electromagnetic field distribution in human head phantom from external source," in *Pcoc. Fifth International Kharkiv Symposium on Physics and Engineering of Microwaves, Millimeter, and Submillimeter Waves MSMW 04*, vol. 2, pp. 838–840, 2004.

[14] K. S. Yee, "Numerical solution of initial boundary value problems involving Maxwell's equations in isotropic media," *IEEE Trans. Antennas Propag.*, vol. 14, pp. 302–307, 1966.

[15] A. Christ, W. Kainz, E. G. Hahn, K. Honegger, M. Zefferer, E. Neufeld, W. Rascher, R. Janka, W. Bautz, J. Chen, B. Kiefer, P. Schmitt, H.-P. Hollenbach, J. Shen, M. Oberle, D. Szczerba, A. Kam, J. W. Guag, and N. Kuster, "The virtual family–development of surface-based anatomical models of two adults and two children for dosimetric simulations," *Phys. Med. Biol.*, vol. 55, pp. 23–38, Jan. 2010.

[16] W. P. Segars, "Development and application of the new dynamic nurbs-based cardiac-torso (NCAT) phantom," Ph.D. dissertation, UNC, 2001.

[17] L. Piegl, "On NURBS: a survey," *IEEE Comput. Graph. Appl.*, vol. 11, no. 1, pp. 55–71, 1991.

[18] Christ, M.-C. Gosselin, M. Christopoulou, S. Kühn, and N. Kuster, "Age-dependent tissue-specific exposure of cell phone users," *Phys. Med. Biol.*, vol. 55, no. 7, p. 1767–1783, 2010.

[19] S. Kühn, W. Jennings, A. Christ, and N. Kuster, "Assessment of induced radio-frequency electromagnetic fields in various anatomical human body models," *Phys Med Biol.*, vol. 54, pp. 875–890, 2009.

[20] M. Parazzini, S. Fiocchi, E. Rossi, A. Paglialonga, and P. Ravazzani, "Transcranial Direct Current Stimulation: Estimation of the Electric Field and of the Current Density in an Anatomical Human Head Model," *IEEE Trans. Biomed. Eng.*, vol. 58, no. 6, pp. 1773–1780, Jun. 2011.

[21] B. Aubert-Broche, A. C. Evans, and L. Collins, "A new improved version of the realistic digital brain phantom," *NeuroImage*, vol. 32, pp. 138–145, Jan. 2006.

[22] C. Gabriel, "Compilation of the dielectric properties of body tissues at RF and microwave frequencies," King's College London, Physics Department, report no. AUOE-TR-1996-0037, June 1996.

[23] P. A. Hasgall, E. Neufeld, M. C. Gosselin, A. Klingenböck and N. Kuster, "IT'IS Database for thermal and electromagnetic parameters of biological tissues," Version 2.4, *www.itis.ethz.ch/database,* July 30th, 2013.

[24] P. Karban, F. Mach, P. Kůs, D. Pánek, and I. Doležel, "Numerical solution of coupled problems using code Agros2D," *Computing*, 2013.

[25] R. J. Meredith, *Engineers' handbook of industrial microwave heating*. London, UK: IET, 1998.

АНАТОМІЧНО РЕАЛІСТИЧНИЙ B-REP ФАНТОМ ГОЛОВИ ЛЮДИНИ ДЛЯ ДОСЛІДЖЕННЯ ЕФЕКТІВ ДВЧ–УВЧ ВИПРОМІНЮВАННЯ

Денис Ніколаєв

Обчислювальні фантоми тіла людини є незамінними інструментами дозиметрії іонізуючих та неіонізуючих випромінювань для розрахунку та оцінки біологічних ефектів опромінення. Окрім того, технології медичної візуалізації та алгоритми реконструкції зображень використовують обчислювальні фантоми для тестування та оптимізації. Метою цього дослідження є розробка нового анатомічно-реалістичного фантома у граничному представленні (B-Rep) для дослідження розподілу фізичних полів у голові людини. Розглянутий алгоритм побудови фантома може бути використаний для автоматизованої розробки фантомів будь-яких суб'єктів досліджень, базуючись на їх скануванні методами медичної візуалізації. Приклад застосування розробленого фантома проілюстрований аналізом розподілу електромагнітного та теплового полів. Розроблений фантом може бути широко застосовуваним у багатьох галузях науки та техніки.

Denys Nikolayev – a postgraduate student of the Department of Theory of Electrical Engineering at the University of West Bohemia (Czech Republic), as well as at the Lviv Polytechnic National University (Ukraine). His research interests include computational electromagnetics, higher order numerical and hybrid methods for RF engineering, coupled problems, and their biomedical applications.